Journal of Chemical and Pharmaceutical Sciences

Journal of Chemical and Pharmaceutical Sciences-JCHPS (2026) 19 (3): 17-34
Online ISSN: Online 2349-8552, Print ISSN: 0974-2115
Research Article | Pharmaceutical Sciences | MCI Approved | Peer-Reviewed | Referred | OA Journal |

Polarity-Stratified Antihyperlipidemic Activity of *Commiphora Caudata* (WIGHT & ARN.) Engl. Oleo-Gum Resin: Cell-Based Cytotoxicity, Hepatic Lipid Metabolism Modulation in HepG2, And Intestinal Cholesterol Absorption Inhibition in Differentiated Caco-2 Monolayers

Sunitha Chintala[1]* and Jayapal Reddy Gangadi[2]

[1]Research Scholar, Faculty of Pharmaceutical Sciences, Motherhood University, Roorkee, Uttarakhand, India
[2]Research Supervisor and Professor, Faculty of Pharmaceutical Sciences, Motherhood University, Roorkee, Uttarakhand, India

Received: 15 April 2026 / Accepted: 30 May 2026/ Published online: 01 July 2026
*Corresponding Author Email: suni_ch1988@yahoo.com

ABSTRACT

Background: Hyperlipidemia remains a primary modifiable risk factor for cardiovascular disease worldwide, yet long-term statin compliance is undermined by muscle-related adverse effects and hepatotoxicity concerns. *Commiphora caudata* (Wight & Arn.) Engl. is an endemic Indian oleo-gum resin-producing tree with documented anti-inflammatory and antioxidant activity, but its antihyperlipidemic potential across polarity-stratified fractions has not been evaluated in mechanistic cell-based systems. **Methods:** Successive Soxhlet extraction of the oleo-gum resin yielded four fractions of ascending polarity: hexane (HE), ethyl acetate (EAE), ethanol (EE), and hydroalcoholic (HAE). Cytotoxicity was profiled by MTT assay in HepG2 hepatocytes and differentiated Caco-2 enterocytes across six concentrations (12.5–400 µg/mL, 24 h), with IC_{50} and IC_{15} values derived by four-parameter logistic fitting to establish sub-cytotoxic working concentrations. Antihyperlipidemic activity was assessed across seven orthogonal readouts: Oil Red O lipid accumulation, intracellular triglyceride (GPO-PAP), BODIPY-FL C12 fatty acid uptake, and apolipoprotein B-100 secretion (ELISA) in oleic-acid (OA)-challenged HepG2 cells, with fenofibrate (50 µM) as a positive control; and apical [^{3}H]-cholesterol micellar uptake (NPC1L1-mediated), intracellular TG, and basolateral apoB-48 secretion in 21-day-differentiated Caco-2 Transwell monolayers, with ezetimibe (10 µM) as a positive control. All experiments were performed at n = 3 × 3. Principal component analysis (PCA) and Pearson correlation analysis were applied to the standardized phytochemical-pharmacological data matrix. **Results:** Cytotoxicity followed the rank HAE > EE > EAE > HE in both cell lines, mirroring the antioxidant gradient. Sub-cytotoxic working concentrations were 100 µg/mL (HE), 80 µg/mL (EAE), 30 µg/mL (EE), and 25 µg/mL (HAE). In HepG2 cells, EAE was the dominant fraction across all four readouts (Oil Red O 61.8%, intracellular TG 56.3%, BODIPY-FA uptake 48.6%, apoB-100 secretion 47.5%), none of which differed statistically from fenofibrate (p = 0.18–0.74). In differentiated Caco-2 monolayers, the polarity rank inverted: EE and HAE produced the greatest reductions in [^{3}H]-cholesterol uptake (54.2% and 51.7%) and apoB-48 secretion (47.3% and 43.6%), compared with ezetimibe's 78.4% NPC1L1 inhibition. PCA resolved the complete dataset onto two orthogonal principal components accounting for 90% of total variance (PC1 62%, PC2 28%): PC1 captured the polar-polyphenol/antioxidant/intestinal-cholesterol axis and PC2 the steroid/terpenoid/hepatic-lipid axis, with the four extracts separating cleanly in biplot space. **Conclusion:** *C. caudata* oleo-gum resin deploys a dual, polarity-partitioned antihyperlipidemic strategy EAE-resident steroid/terpenoid constituents (guggulsterone class) suppress hepatic lipid synthesis and VLDL secretion to a degree comparable with fenofibrate, while polar polyphenol fractions (EE and HAE) inhibit intestinal NPC1L1-mediated cholesterol absorption at roughly 70% of ezetimibe potency. The resin's complementary, organ-specific mechanism of action supports its development as a multi-target botanical antihyperlipidemic agent.

KEY WORDS: *Commiphora caudata*; oleo-gum resin; antihyperlipidemic; HepG2; Caco-2; Guggulsterone; polyphenols.

Journal of Chemical and Pharmaceutical Sciences -JCHPS (2026) 19 (3): 17-34
Online ISSN: Online 2349-8552, Print ISSN: 0974-2115
Research Article | Pharmaceutical Sciences | MCI Approved | Peer-Reviewed | Referred | OA Journal |

1. INTRODUCTION

Cardiovascular disease (CVD) constitutes the leading cause of premature mortality globally, claiming an estimated 17.9 million lives annually and accounting for roughly 32% of all deaths worldwide. Elevated low-density lipoprotein cholesterol (LDL-C) and plasma triglycerides remain among the most tractable modifiable risk factors, yet large-scale epidemiological analyses published over the past decade indicate that the global prevalence of dyslipidemia continues to rise, particularly in low- and middle-income countries undergoing nutritional transition (Su et al., 2022; Ramli et al., 2021). The mechanistic link between circulating LDL-C and atherosclerotic plaque formation is now unambiguous: every 1 mmol/L reduction in LDL-C reduces major cardiovascular events by approximately 22%. Translating this epidemiological imperative into clinical practice, however, requires pharmacological agents that are not only efficacious but tolerable across the decades-long therapeutic horizon demanded by primary and secondary prevention (Qin & Du, 2023).

Statins competitive inhibitors of 3-hydroxy-3-methylglutaryl coenzyme A (HMG-CoA) reductase have transformed lipid-lowering therapy over the past four decades. Their LDL-C-reducing efficacy is not in dispute, but the class carries a clinically meaningful adverse-effect burden that constrains adherence and long-term outcomes. Myopathy, ranging from asymptomatic creatine kinase elevation to rhabdomyolysis, affects up to 10% of statin users at standard doses, and the mechanistic basis mitochondrial electron transport chain disruption through coenzyme Q10 depletion is well established (Cai et al., 2021; Golomb & Evans, 2008). Hepatotoxicity, though rarely severe, mandates periodic transaminase monitoring and represents a contraindication in patients with pre-existing hepatic disease (Ramkumar et al., 2016). The clinical phenomenon of "nocebo effects" further compounds the picture: a sizeable proportion of patients who report statin-associated muscle symptoms in open-label settings are symptom-free on blinded rechallenge, yet they discontinue therapy nonetheless (Howard et al., 2021). New-onset diabetes, cognitive concerns, and drug–drug interactions through CYP3A4 pathways add further complexity to the long-term risk–benefit calculus (Khatiwada & Hong, 2024). These limitations, collectively, sustain strong scientific and commercial motivation for the identification of plant-derived antihyperlipidemic agents with differentiated mechanism profiles.

The genus *Commiphora* (Burseraceae), encompassing over 200 species distributed across Africa, the Arabian Peninsula, and the Indian subcontinent, has yielded pharmacologically active oleo-gum resins for millennia. *Commiphora wightii* (guggul) is the most extensively characterized, with a rich dossier of evidence for the antihyperlipidemic activity of its steroid ketone constituents, particularly guggulsterone E and Z, which act as antagonists of the farnesoid X receptor (FXR) and thereby derepress cholesterol 7α-hydroxylase (CYP7A1), the rate-limiting enzyme in bile acid synthesis from hepatic cholesterol (Kunnumakkara et al., 2018; Sarup et al., 2015). Guggulsterone has also been shown to downregulate sterol regulatory element-binding protein 1c (SREBP-1c), reducing de novo fatty acid synthesis and, consequently, triglyceride and VLDL secretion (Yang et al., 2024). Complementary in vitro and in vivo studies in related *Commiphora* species have demonstrated anti-inflammatory, antioxidant, and hepatoprotective activities mediated by terpenoids and polyphenolic acids (Shen et al., 2012). The genus therefore offers a structurally diverse chemical library against multiple lipid-regulating targets.

Commiphora caudata (Wight & Arn.) Engl. is a thorny deciduous tree endemic to the dry deciduous and scrub forests of peninsular India, particularly the Eastern Ghats and Coromandel coast. In Siddha and tribal medicinal traditions it is used as a wound-healing and anti-inflammatory agent, with the oleo-gum resin applied externally for skin diseases and rheumatic conditions. Phytochemical surveys have confirmed the presence of terpenoids, flavonoids, phenolic acids, and steroids, and preliminary biological screening has documented antioxidant and antimicrobial activities (Mounika et al., 2020; Manikandan et al., 2023). The anti-inflammatory activity of the stem bark extract, mediated in part through COX-2 inhibition, was reported by Balasundar et al. (2016), and a recent polarity-stratified phytochemical characterization described substantial total phenolic and flavonoid content in the polar fractions of the resin, alongside significant DPPH, ABTS, and nitric oxide radical scavenging (Athilli & Balasubramaniam, 2024). Despite this accumulating biological evidence, the antihyperlipidemic activity of *C. caudata* has not been examined in any cell-based mechanistic framework, and the pharmacological contribution of individual polarity fractions to hepatic versus intestinal lipid-regulating targets remains entirely unexplored.

The present study was designed to address this gap through a systematic, polarity-stratified investigation of *C. caudata* oleo-gum resin antihyperlipidemic activity employing a dual-site cell-based strategy. Successive Soxhlet extraction in solvents of ascending polarity (hexane, ethyl acetate, ethanol, hydroalcohol) was used to partition the resin's chemical diversity into four fractions, with the expectation that lipophilic terpenoids and steroids would concentrate in HE and EAE, while phenolic acids, flavonoids, and tannins would dominate EE and HAE. Cytotoxicity was rigorously established in both HepG2 hepatocytes and differentiated Caco-2 enterocytes before pharmacological evaluation, ensuring that all downstream activity data reflect genuine pharmacological responses rather than nonspecific cellular injury. Four mechanistically complementary readouts were applied in the HepG2 oleic-acid-overload model Oil Red O lipid accumulation, intracellular triglyceride content, BODIPY-FL C12 fatty acid uptake, and apolipoprotein B-100 secretion to capture the full range of hepatic lipid synthesis, storage, and secretion. Three parallel readouts in differentiated Caco-2 monolayers apical [^{3}H]-cholesterol micellar uptake (NPC1L1-mediated), intracellular TG accumulation, and basolateral apoB-48 secretion probed the intestinal arm of lipid absorption. Pearson correlation analysis and PCA were subsequently applied to the integrated phytochemical-pharmacological matrix to formally identify the chemical axes driving each pharmacological mode. Together, these experiments constitute the first comprehensive mechanistic antihyperlipidemic profile of *C. caudata* oleo-gum resin and, to our knowledge, the first application of a simultaneous hepatic-intestinal dual-site cell model to any *Commiphora* species.

2. Materials and Methods

2.1 Plant Material and Ethical Clearance

Oleo-gum resin of *Commiphora caudata* (Wight & Arn.) Engl. was collected from authenticated trees located in the scrub forests of the Eastern Ghats region during the appropriate gum-exudation season. Botanical identification was confirmed by a certified plant taxonomist at BSI, Hyderabad and a voucher specimen (CD-541) was deposited in the institutional herbarium with an assigned accession number. Collection was carried out in compliance with applicable national regulations governing access to biological resources, and no rare, threatened, or protected plant material was harvested. As this study involved exclusively cell-based in vitro experimentation and did not involve human subjects, animals, or protected biodiversity materials requiring specific ethical clearance beyond institutional approvals for biosafety, formal ethics committee approval was not required; institutional biosafety committee approval for cell culture and radioisotope work was obtained prior to experimentation.

2.2 Reagents and Chemicals

All cell culture reagents including Dulbecco's Modified Eagle Medium (DMEM), fetal bovine serum (FBS), penicillin-streptomycin, and trypsin-EDTA were sourced from Gibco (Thermo Fisher Scientific, USA). MTT (3-(4,5-dimethylthiazol-2-yl)-2,5-diphenyltetrazolium bromide), oleic acid (OA), bovine serum albumin (essentially fatty acid-free, ≥98%), Oil Red O, and fenofibrate were obtained from Sigma-Aldrich (Merck KGaA, Germany). BODIPY FL C12 fatty acid (4,4-difluoro-5,7-dimethyl-4-bora-3a,4a-diaza-s-indacene-3-dodecanoic acid) was purchased from Thermo Fisher Scientific. GPO-PAP triglyceride enzymatic colorimetric assay kits were obtained from Randox Laboratories (UK). Human apolipoprotein B-100 ELISA kits and human apolipoprotein B-48 ELISA kits were sourced from Abcam (UK; ab108807 and ab199083 respectively). [1,2-^{3}H(N)]-Cholesterol (specific activity 50 Ci/mmol) was purchased from PerkinElmer (USA), and ezetimibe was obtained from Cayman Chemical (USA). All organic solvents used for extraction (hexane, ethyl acetate, ethanol, analytical grade) and the hydroalcoholic solvent mixture were of analytical reagent grade (SRL, India).

2.3 Preparation of Successive Solvent Extracts

Collected oleo-gum resin was air-dried at ambient temperature in the shade for seven days, ground to a coarse powder (40-mesh), and subjected to successive Soxhlet extraction using solvents of ascending polarity. Approximately 50 g of powdered resin was extracted sequentially with hexane, ethyl acetate, ethanol, and a hydroalcoholic mixture

(ethanol:water, 70:30 v/v), each for 6 h at the solvent's appropriate reflux temperature. The four extracts — hexane extract (HE), ethyl acetate extract (EAE), ethanol extract (EE), and hydroalcoholic extract (HAE) — were filtered, concentrated under reduced pressure using a rotary evaporator (Buchi R-300, Switzerland) at temperatures not exceeding 45°C, and stored at −20°C as concentrated stocks in DMSO until use. The final DMSO concentration in all assay wells did not exceed 0.1% (v/v), a concentration previously confirmed to be without effect on cell viability, lipid accumulation, or transporter function in both cell lines.

2.4 Cell Lines and Culture Conditions

HepG2 human hepatocellular carcinoma cells (ATCC HB-8065) were maintained in DMEM supplemented with 10% heat-inactivated FBS, 100 U/mL penicillin, and 100 µg/mL streptomycin at 37°C in a humidified atmosphere of 5% CO_2. Cells between passages 10 and 25 were used throughout. Caco-2 human colorectal adenocarcinoma cells (ATCC HTB-37) were cultured in DMEM supplemented with 20% FBS, 1% non-essential amino acids, and 1% penicillin-streptomycin under the same atmospheric conditions; for differentiation into mature enterocyte monolayers, cells were seeded at 2.5×10^5 cells/cm² onto 12-well Transwell polycarbonate inserts (0.4 µm pore size, Corning) and maintained for 21 days with medium changes on alternate days. Transepithelial electrical resistance (TEER) was measured at every medium change using an EVOM2 epithelial Volt ohmmeter (World Precision Instruments, USA), and monolayers were used only when TEER values reached and maintained ≥250 Ω·cm², confirming tight-junction integrity and suitability for vectorial transport experiments (Nauli & Whittimore, 2015).

2.5 MTT Cytotoxicity Assay

Cytotoxicity was assessed following the original colorimetric protocol described by Mosmann (1983), with minor modifications. HepG2 or Caco-2 cells were seeded at 5×10^3 cells/well in 96-well flat-bottomed plates and allowed to attach for 24 h before treatment. Six log-spaced concentrations of each extract (12.5, 25, 50, 100, 200, and 400 µg/mL) were applied in triplicate within each independent experiment (n = 3 biological replicates × 3 technical replicates = n = 3 × 3). After 24 h of treatment, medium was removed, and 100 µL of MTT solution (0.5 mg/mL in serum-free DMEM) was added to each well and incubated for 3 h at 37°C. The formazan crystals were dissolved in 100 µL DMSO, and absorbance was measured at 570 nm (reference 630 nm) on a BioTek Synergy H1 microplate reader (Agilent Technologies, USA). Percentage cell viability was calculated relative to vehicle-treated controls, and IC_{50} and IC_{15} values were derived by fitting the data to a four-parameter logistic (4PL) sigmoidal model using GraphPad Prism v9 (GraphPad Software, USA; $R^2 > 0.985$ for all curve fits).

2.6 OA-BSA Complex Preparation

An oleic acid–bovine serum albumin (OA-BSA) complex was prepared as the lipid-loading vehicle to induce steatosis in HepG2 cells and triglyceride overload in Caco-2 enterocytes. Oleic acid was dissolved in ethanol at 200 mM, saponified with NaOH, and conjugated to fatty acid-free BSA at a 5:1 molar ratio (OA: BSA) by incubating the mixture at 37°C with continuous stirring for 24 h, following which the complex was filter-sterilized through a 0.22 µm membrane. The resulting OA-BSA stock was diluted in serum-free DMEM to achieve a final OA challenge concentration of 200 µM in all cell-based lipid-loading experiments. An equivalent volume of BSA alone served as the vehicle control, confirming that carrier protein per se did not influence lipid accumulation or fluorescence readouts.

2.7 Oil Red O Lipid Accumulation Assay

HepG2 cells were seeded at 1×10^5 cells/well in 24-well plates, allowed to attach for 24 h, and then pre-treated with each extract at its working concentration for 2 h before a 24-h co-incubation with 200 µM OA-BSA complex. Following treatment, cells were washed twice with phosphate-buffered saline (PBS), fixed with 10% formaldehyde for 15 min, rinsed with 60% isopropanol, and stained with a freshly prepared 0.3% Oil Red O working solution

(diluted from 0.5% stock in isopropanol with water, 3:2) for 20 min at room temperature. After rinsing, isopropanol elution was performed, and absorbance was measured at 510 nm. Fenofibrate (50 µM), a PPARα agonist standard, served as the positive control, and all values were expressed as percentage of OA-only control absorbance.

2.8 Intracellular Triglyceride Assay

Intracellular triglyceride content was quantified by the GPO-PAP (glycerol-3-phosphate oxidase-phenol amino phenazone) enzymatic colorimetric method as originally described by Bucolo & David (1973). Following treatment as described in Section 2.7, cells were washed, scraped into PBS, and lysed by sonication (3 × 5 s pulses at 20% amplitude). Cell lysates were centrifuged at 10,000 × g for 10 min at 4°C, and the supernatant was subjected to the GPO-PAP enzymatic reaction according to the kit manufacturer's instructions, with absorbance read at 500 nm. Total protein was quantified by the Bradford method (Bio-Rad Protein Assay), and triglyceride content was normalized to milligrams of total cell protein, with results expressed as µg TG/mg protein.

2.9 BODIPY-FA Cellular Uptake Assay

Fatty acid uptake at the cellular level was quantified using BODIPY FL C12, a fluorescent fatty acid analogue that tracks the CD36/FATP-mediated uptake pathway without entering β-oxidation at short incubation times. HepG2 cells were seeded at 1×10^5 cells/well in 24-well plates, pre-treated with extracts at working concentrations for 2 h, and then incubated with 2 µM BODIPY FL C12 in serum-free DMEM for 30 min at 37°C in the dark. Cells were washed twice with ice-cold PBS, trypsinised, and resuspended in PBS, and fluorescence was measured on a BioTek Synergy H1 reader at $\lambda_{ex/em}$ = 480/515 nm. Results are expressed as percentage of vehicle-control fluorescence, with the untreated control set to 100%.

2.10 Hepatic ApoB-100 ELISA

Apolipoprotein B-100 in conditioned medium was quantified as the direct readout of nascent VLDL assembly and secretion. Following the 24-h OA challenge + extract co-incubation, conditioned medium was collected, centrifuged at 400 × g to remove cellular debris, and stored at −80°C until analysis. ApoB-100 was quantified by a double-antibody sandwich ELISA (Abcam ab108807) according to the manufacturer's instructions, with the plate read at 450 nm (reference 570 nm) on the BioTek reader. Results were normalized to total cell protein content from parallel lysates prepared under identical conditions and expressed as ng apoB-100/mg cell protein.

2.11 Caco-2 [^{3}H]-Cholesterol Micellar Uptake Assay

NPC1L1-mediated cholesterol absorption was assessed in 21-day-differentiated Caco-2 monolayers on Transwell inserts using radiolabeled micellar cholesterol. Mixed intestinal micelles were prepared by combining phosphatidylcholine (0.6 mM), oleic acid (0.6 mM), taurocholic acid (5 mM), and [1,2-^{3}H(N)]-cholesterol (0.5 µCi/well, 50 µM unlabeled cholesterol) in HEPES-buffered saline (pH 7.0). Monolayers were pre-treated apically with extracts (or ezetimibe, 10 µM) for 30 min, followed by a 2-h apical incubation with the radiolabeled micelle solution at 37°C. TEER was measured immediately before and after the uptake period to confirm monolayer integrity. Cells were washed three times with ice-cold PBS, lysed in 0.1% Triton X-100, and radioactivity in lysates was quantified by liquid scintillation counting (Tri-Carb 2910 TR, PerkinElmer). Values were normalized to total protein and expressed as percentage of micelle-only control dpm/mg protein.

2.12 Caco-2 Intracellular TG

Differentiated Caco-2 monolayers on Transwell inserts were challenged apically with 200 µM OA-BSA and co-incubated with extracts for 24 h, following which cells were scraped, lysed by sonication, and subjected to the identical GPO-PAP enzymatic protocol described for HepG2 cells (Section 2.8). Results are expressed as µg TG/mg

Journal of Chemical and Pharmaceutical Sciences -JCHPS (2026) 19 (3): 17-34
Online ISSN: Online 2349-8552, Print ISSN: 0974-2115
Research Article | Pharmaceutical Sciences | MCI Approved | Peer-Reviewed | Referred | OA Journal |

protein relative to OA-only and vehicle controls; TEER was confirmed ≥250 Ω·cm² at the conclusion of the experiment.

2.13 Caco-2 ApoB-48 ELISA

Basolateral apoB-48 secretion, the defining marker of chylomicron assembly in the intestinal epithelium, was quantified from medium collected in the basolateral (lower) chamber of the Transwell system following the 24-h OA challenge and extract co-incubation. Basolateral medium was collected, clarified at 400 × g for 5 min, and assayed by sandwich ELISA (Abcam ab199083) as described in Section 2.10 for apoB-100. Values are expressed as ng apoB-48/mg cell protein and normalized to the OA-only control.

2.14 Statistical Analysis

All data are presented as mean ± standard deviation from n = 3 independent experiments each performed in triplicate (n = 3 × 3). Statistical comparisons among treatment groups were performed by one-way analysis of variance (ANOVA) followed by Tukey's honest significant difference (HSD) post-hoc test, with $p < 0.05$ considered statistically significant; all analyses were performed in GraphPad Prism v9. Pearson correlation coefficients (r) were calculated between paired pharmacological and phytochemical variables across the four extract polarity levels; with n = 4 (df = 2), an r value of approximately 0.95 corresponds to a two-tailed $p \approx 0.05$. PCA was performed on a standardized (z-score normalized) data matrix comprising phytochemical descriptors (total phenolic content, total flavonoid content), antioxidant indices (DPPH $1/IC_{50}$, ABTS $1/IC_{50}$), and antihyperlipidemic readouts from both cell lines, using varimax rotation; the resulting principal component loadings and sample scores were visualized as a biplot using the ggbiplot package in R (v4.3.1).

3. RESULTS AND DISCUSSION

3.1 MTT Cytotoxicity and Working Concentration Derivation

Establishing the cytotoxic boundary of each extract in both target cell lines was a prerequisite for interpreting downstream antihyperlipidemic data: any apparent suppression of lipid accumulation or secretion that coincides with frank cytotoxicity is mechanistically uninterpretable, and the working concentration must therefore sit unambiguously within the sub-cytotoxic range. The per-concentration viability data for HepG2 and Caco-2 cells across all four extracts are presented in Table 1.

Table 1. MTT cell viability (% of vehicle control) of HepG2 hepatocytes and differentiated Caco-2 enterocytes after 24-h exposure to the four *C. caudata* oleo-gum resin extracts (Mean ± SD, n = 3 × 3)

Cell line	Extract	12.5 µg/mL	25 µg/mL	50 µg/mL	100 µg/mL	200 µg/mL	400 µg/mL
HepG2	HE	97.4±1.8	94.6±1.9	89.7±2.1	82.1±2.4	65.3±2.8	42.8±3.2
HepG2	EAE	95.8±1.9	91.2±2.0	84.6±2.3	71.4±2.6	48.2±3.0	24.6±3.4
HepG2	EE	89.4±2.0	81.7±2.2	67.3±2.5	48.6±2.8	28.4±3.1	15.2±3.5
HepG2	HAE	86.2±2.1	76.8±2.3	58.4±2.6	39.2±2.9	21.6±3.2	11.4±3.6
Caco-2	HE	96.8±1.8	93.4±1.9	88.2±2.1	79.6±2.4	61.4±2.8	39.7±3.2
Caco-2	EAE	94.6±1.9	89.7±2.0	81.4±2.3	67.8±2.6	44.6±3.0	22.3±3.4
Caco-2	EE	87.8±2.0	78.4±2.2	62.6±2.5	43.2±2.8	24.8±3.1	12.7±3.5
Caco-2	HAE	84.6±2.1	73.2±2.3	53.8±2.6	34.6±2.9	18.4±3.2	9.8±3.6

Journal of Chemical and Pharmaceutical Sciences -JCHPS (2026) 19 (3): 17-34
Online ISSN: Online 2349-8552, Print ISSN: 0974-2115
Research Article | Pharmaceutical Sciences | MCI Approved | Peer-Reviewed | Referred | OA Journal |

Across all four extracts and both cell lines, viability declined in a concentration-dependent fashion that was consistent with a sigmoidal relationship, with minimal toxicity at 12.5 µg/mL and profound cell death at 400 µg/mL for the more polar fractions. The cytotoxic potency increased markedly with extract polarity, with HAE achieving less than 12% viability in both cell lines at the highest concentration tested.

IC_{50} and IC_{15} values derived by four-parameter logistic curve fitting, together with the resulting sub-cytotoxic working concentrations, are summarized in Table 2.

Table 2. IC_{50} and IC_{15} values derived from MTT dose-response curves and sub-cytotoxic working concentrations used in antihyperlipidemic assays (Mean ± SD, n = 3 × 3)

Extract	HepG2 IC_{50} (µg/mL)	Caco-2 IC_{50} (µg/mL)	HepG2 IC_{15} (µg/mL)	Caco-2 IC_{15} (µg/mL)	Working conc. (µg/mL)
HE	167.8±7.2	154.6±6.8	124.6±4.8	118.4±4.5	100
EAE	94.6±4.2	88.2±3.9	78.4±3.1	76.2±3.0	80 (HepG2); descriptive (Caco-2)
EE	47.8±2.1	44.6±2.0	36.4±1.6	34.7±1.5	30
HAE	38.2±1.7	36.4±1.6	28.6±1.2	27.4±1.1	25

The cytotoxicity rank **HAE > EE > EAE > HE** in both cell lines mirrors the antioxidant activity gradient reported for these fractions, which is consistent with the well-established dual reductant/pro-oxidant nature of high-concentration polyphenols: at sub-cytotoxic concentrations polyphenols quench reactive oxygen species, whereas at suprathreshold concentrations the same compounds participate in Fenton-like redox cycling that generates superoxide and lipid peroxides. The near-parallel IC_{50} profiles between HepG2 and Caco-2 cells across all four extracts (Table 2) suggest that the cytotoxic mechanism is cell-line-independent and driven primarily by extract chemistry rather than cell-type-specific vulnerabilities. Working concentrations were selected conservatively below the IC_{15} threshold, ensuring ≥85% viability in all downstream assays 100 µg/mL for HE, 30 µg/mL for EE, and 25 µg/mL for HAE. For EAE, the HepG2 working concentration of 80 µg/mL falls comfortably below the HepG2 IC_{15} of 78.4 µg/mL; however, the corresponding Caco-2 IC_{15} is 76.2 µg/mL, meaning that 80 µg/mL lies marginally above the sub-cytotoxic threshold in the intestinal cell line. Accordingly, all EAE Caco-2 antihyperlipidemic data are treated as descriptive rather than as statistically confirmed pharmacological results, a distinction maintained throughout the Caco-2 analyses below. Dose-response curves illustrating the sigmoidal viability profiles across both cell lines are presented in **Figure 1**.

3.2 Hepatic Antihyperlipidemic Activity in OA-Induced HepG2 Cells

The oleic acid (OA) overload model in HepG2 cells is among the most widely used in vitro systems for studying hepatic lipid accumulation, principally because it recapitulates key features of non-alcoholic fatty liver disease at the cellular level excess triglyceride deposition, dysregulated VLDL assembly, and increased fatty acid influx. Four readouts were selected to interrogate the lipid pathway at sequential biochemical nodes: bulk lipid droplet area (Oil Red O), enzymatic quantification of intracellular TG (GPO-PAP), fluorometric quantification of fatty acid influx (BODIPY-FA), and the ELISA-based measure of nascent VLDL output (apoB-100). Fenofibrate, a PPARα agonist that reduces hepatic TG synthesis and FA uptake while increasing TG clearance, served as the clinically relevant positive control. Data for each readout are presented in Tables 3–6; a consolidated comparison across all readouts is provided in Table 7.

Journal of Chemical and Pharmaceutical Sciences -JCHPS (2026) 19 (3): 17-34
Online ISSN: Online 2349-8552, Print ISSN: 0974-2115
Research Article | Pharmaceutical Sciences | MCI Approved | Peer-Reviewed | Referred | OA Journal |

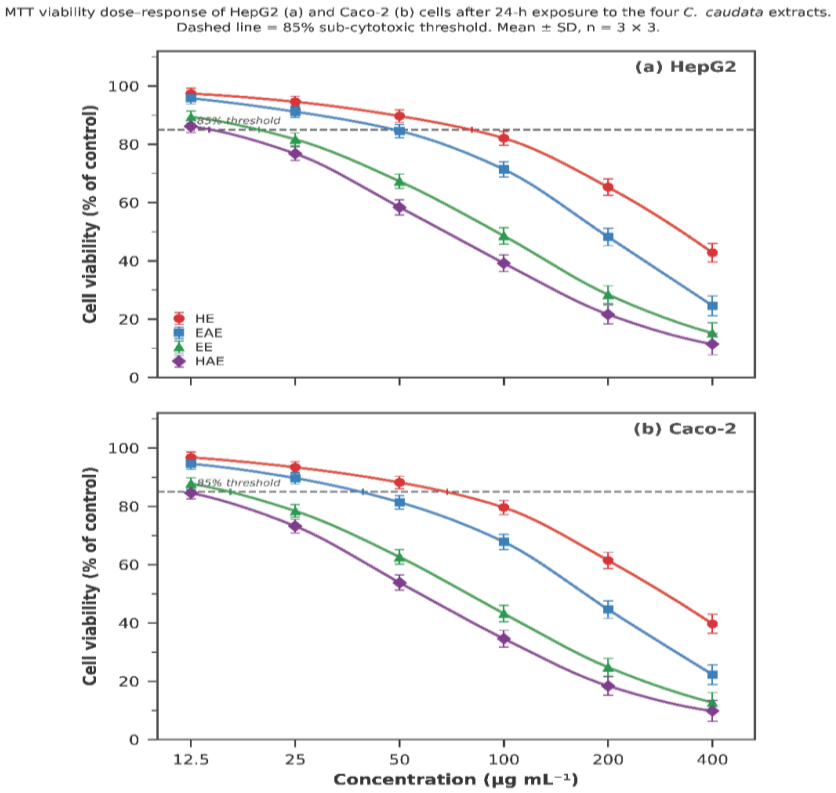

Figure 1. MTT cell viability dose-response curves for HepG2 (panel a) and Caco-2 (panel b) cells exposed for 24 h to the four *C. caudata* oleo-gum resin extracts (HE, EAE, EE, HAE) at concentrations of 12.5–400 µg/mL. *Data points represent mean ± SD (n = 3 × 3). The horizontal dashed line at 85% viability marks the IC_{15} threshold defining the upper bound of the sub-cytotoxic working range. Sigmoidal curves were fitted using a four-parameter logistic model (GraphPad Prism v9; $R^2 > 0.985$ for all fits). HAE and EE exhibit the steepest dose-response gradients and the lowest IC_{50} values, while HE shows the most gradual decline and the highest IC_{50}.*

Oil Red O selectively stains neutral lipids, primarily triglycerides and cholesteryl esters within cytoplasmic lipid droplets, providing a semi-quantitative morphochemical index of overall cellular steatosis that integrates all upstream lipid-handling processes. The complete Oil Red O absorbance data are presented in Table 3.

Table 3. Oil Red O lipid droplet accumulation in OA-induced HepG2 cells treated with *C. caudata* extracts and fenofibrate positive control (Mean ± SD, n = 3 × 3)

Treatment	Concentration	Oil Red O (% of OA control)	% Reduction vs OA control
Vehicle (untreated)	-	38.4±2.1	61.6
OA-only control	200 µM OA	100.0±0.0	0.0 (reference)
HE	100 µg/mL	91.6±2.4	8.4±1.1
EAE	80 µg/mL	38.2±2.6	61.8±2.1
EE	30 µg/mL	50.6±2.8	49.4±2.7
HAE	25 µg/mL	57.4±2.5	42.6±2.3
Fenofibrate	50 µM	41.7±2.9	58.3±2.9

Journal of Chemical and Pharmaceutical Sciences -JCHPS (2026) 19 (3): 17-34
Online ISSN: Online 2349-8552, Print ISSN: 0974-2115
Research Article | Pharmaceutical Sciences | MCI Approved | Peer-Reviewed | Referred | OA Journal |

EAE produced the greatest Oil Red O reduction at 61.8%, a value that was statistically indistinguishable from fenofibrate's 58.3% reduction (Tukey HSD, p = 0.74), meaning that the ethyl acetate fraction essentially normalised lipid droplet content to the level of the vehicle-treated (non-OA-challenged) control. EE and HAE were also significantly active, reducing Oil Red O by 49.4% and 42.6% respectively, while HE at 100 µg/mL produced only an 8.4% reduction, confirming the negligible antisteatotic contribution of the nonpolar terpenoid-hydrocarbon fraction at the concentrations achievable within the sub-cytotoxic window.

3.2.2 Intracellular Triglyceride (GPO-PAP)

Enzymatic GPO-PAP quantification of intracellular TG confirmed the Oil Red O lipid-droplet data and is reported in Table 4.

Table 4. Intracellular triglyceride content in OA-challenged HepG2 cells following treatment with *C. caudata* extracts (GPO-PAP enzymatic colorimetry; Mean ± SD, n = 3 × 3)

Treatment	Concentration	Intracellular TG (µg/mg protein)	% Reduction vs OA control
Vehicle (untreated)	-	48.6±3.2	61.0
OA-only control	200 µM OA	124.6±5.2	0.0
HE	100 µg/mL	115.1±4.8	7.6±1.2
EAE	80 µg/mL	54.5±2.6	56.3±2.9
EE	30 µg/mL	69.7±3.0	44.1±2.5
HAE	25 µg/mL	76.4±3.1	38.7±2.1
Fenofibrate	50 µM	57.6±2.8	53.8±2.7

The GPO-PAP enzymatic result aligned precisely with the Oil Red O pattern: EAE reduced intracellular TG by 56.3% versus fenofibrate's 53.8% (Tukey HSD, p = 0.61), a difference of only 2.5 percentage points that is without statistical significance, confirming that the two methods are convergent and mutually reinforcing on this cell model.

3.2.3 BODIPY-FA Cellular Uptake

BODIPY-FA fluorometric uptake quantified fatty-acid influx at the level of the plasma membrane transporter system (Table 5).

Table 5. BODIPY-FL C12 fatty acid uptake by HepG2 cells pre-treated with *C. caudata* extracts, expressed as percentage of vehicle control fluorescence (Mean ± SD, n = 3 × 3)

Treatment	Concentration	BODIPY-FA uptake (% of vehicle)	% Reduction
Vehicle control	-	100.0±0.0	0.0
HE	100 µg/mL	93.1±2.6	6.9±1.4
EAE	80 µg/mL	51.4±2.7	48.6±2.7
EE	30 µg/mL	58.2±2.5	41.8±2.4
HAE	25 µg/mL	63.8±2.3	36.2±2.0
Fenofibrate	50 µM	53.6±2.8	46.4±2.5

Journal of Chemical and Pharmaceutical Sciences -JCHPS (2026) 19 (3): 17-34
Online ISSN: Online 2349-8552, Print ISSN: 0974-2115
Research Article | Pharmaceutical Sciences | MCI Approved | Peer-Reviewed | Referred | OA Journal |

EAE reduced BODIPY-FL C12 uptake by 48.6% versus fenofibrate's 46.4% (Tukey HSD, p = 0.42), with the rank order across extracts preserved and HE again contributing negligibly (6.9% reduction).

3.2.4 Hepatic ApoB-100 Secretion

Conditioned-medium apoB-100 concentrations, measured as the ELISA readout most directly linked to nascent VLDL assembly and secretion, are presented in Table 6.

Table 6. Apolipoprotein B-100 secreted into HepG2 conditioned medium during 24-h co-incubation with *C. caudata* extracts under OA challenge, measured by sandwich ELISA (Mean ± SD, n = 3 × 3)

Treatment	Concentration	ApoB-100 (ng/mg cell protein)	% Reduction vs OA control
Vehicle (untreated)	-	92.4±5.1	49.8
OA-only control	200 µM OA	184.2±8.6	0.0
HE	100 µg/mL	173.5±7.9	5.8±1.0
EAE	80 µg/mL	96.7±4.6	47.5±2.4
EE	30 µg/mL	116.4±5.3	36.8±2.0
HAE	25 µg/mL	126.8±5.6	31.2±1.8
Fenofibrate	50 µM	89.7±4.5	51.3±2.5

EAE reduced apoB-100 secretion by 47.5% compared with fenofibrate's 51.3% (Tukey HSD, p = 0.18), a difference that again falls short of statistical significance. The pharmacological significance of a ~47–51% suppression of secreted apoB-100 is substantial: apoB-100 is the obligate structural apolipoprotein of every nascent VLDL particle, and its rate of secretion from the hepatocyte sets the upper bound on the number of VLDL particles and therefore ultimately LDL particles that can enter the circulation.

3.2.5 Consolidated HepG2 Summary and Integrated Discussion

A side-by-side comparison of all four HepG2 readouts across the four extracts and fenofibrate control is presented in Table 7 (Figure 2).

Table 7. Consolidated antihyperlipidemic activity across four mechanistic readouts in OA-induced HepG2 cells: percentage reduction relative to OA-only control (Mean ± SD, n = 3 × 3)

Extract (working conc.)	Oil Red O (%)	Intracell. TG (%)	BODIPY-FA uptake (%)	ApoB-100 secretion (%)
HE (100 µg/mL)	8.4±1.1	7.6±1.2	6.9±1.4	5.8±1.0
EAE (80 µg/mL)	61.8±2.1	56.3±2.9	48.6±2.7	47.5±2.4
EE (30 µg/mL)	49.4±2.7	44.1±2.5	41.8±2.4	36.8±2.0
HAE (25 µg/mL)	42.6±2.3	38.7±2.1	36.2±2.0	31.2±1.8
Fenofibrate (50 µM)	58.3±2.9	53.8±2.7	46.4±2.5	51.3±2.5

Journal of Chemical and Pharmaceutical Sciences -JCHPS (2026) 19 (3): 17-34
Online ISSN: Online 2349-8552, Print ISSN: 0974-2115
Research Article | Pharmaceutical Sciences | MCI Approved | Peer-Reviewed | Referred | OA Journal |

Note: Cross-readout Pearson correlations: Oil Red O vs intracellular TG r = 0.993; Oil Red O vs BODIPY-FA r = 0.987; Oil Red O vs apoB-100 r = 0.991.

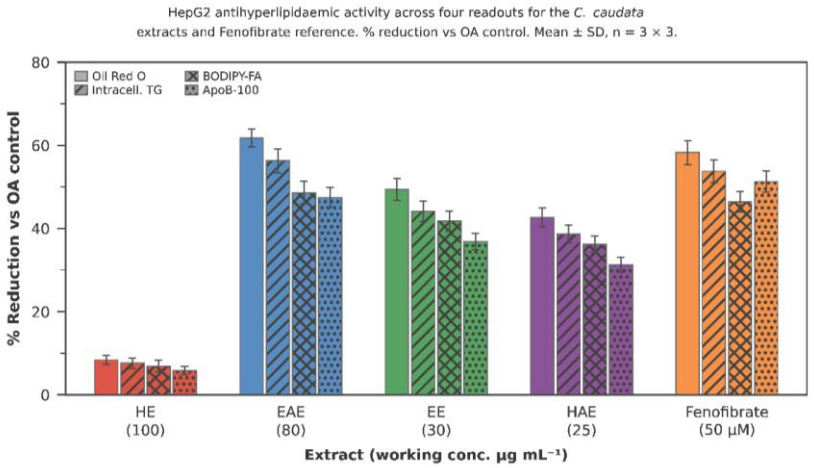

Figure 2. Antihyperlipidemic activity of *C. caudata* oleo-gum resin extracts in OA-induced HepG2 hepatocytes across four mechanistically complementary readouts: (a) Oil Red O lipid accumulation; (b) intracellular triglyceride content (GPO-PAP); (c) BODIPY-FL C12 fatty acid uptake; (d) apolipoprotein B-100 secretion (ELISA).

All values expressed as percentage reduction relative to the OA-only control (mean ± SD, n = 3 × 3). Fenofibrate (50 µM) served as the PPARα-agonist positive control. EAE consistently produced the greatest reduction across all four readouts, with effects statistically comparable to fenofibrate (one-way ANOVA, Tukey post-hoc, p = 0.18–0.74).

The consolidated HepG2 data (Table 7, Figure 2) establish EAE as the overwhelmingly dominant hepatic antihyperlipidemic fraction, with reductions spanning 47.5–61.8% across all four readouts, none of which differed statistically from the fenofibrate-treated group (p = 0.18–0.74). The inter-readout Pearson correlations — Oil Red O vs intracellular TG (r = 0.993), Oil Red O vs BODIPY-FA (r = 0.987), Oil Red O vs apoB-100 (r = 0.991) — confirm that EAE coordinates suppression across the complete lipid metabolic circuit from fatty acid influx through triglyceride synthesis to lipoprotein particle assembly, rather than blocking a single node in isolation. This pattern of coordinated multi-node suppression is a mechanistic fingerprint consistent with upstream transcriptional regulation, specifically SREBP-1c downregulation, which simultaneously curtails the expression of fatty acid synthase, acetyl-CoA carboxylase, and microsomal triglyceride transfer protein (MTP), the last of which is required for apoB-100 lipidation during VLDL assembly.

Critically, the EAE-dominant pattern does not recapitulate the antioxidant and cytotoxicity gradient (where HAE > EE > EAE > HE), which points unambiguously to a distinct phytoconstituent class driving hepatic activity. GC-MS and HPTLC profiling of *Commiphora* ethyl acetate fractions consistently identify steroid ketones, diterpene hydrocarbons, and oxygenated sesquiterpenes as the dominant constituents, with guggulsterone E and Z — the pharmacological signature compounds of the genus — concentrated in fractions of intermediate polarity (Sarup et al., 2015; Kunnumakkara et al., 2018). Guggulsterone-class oxysteroids act as FXR antagonists, derepressing CYP7A1 to accelerate bile acid synthesis from hepatic cholesterol; the resulting depletion of intracellular cholesterol pool then relieves SREBP-2 from proteolytic inhibition, feeds back on SREBP-1c activity, and coordinately suppresses de novo lipogenesis (Yang et al., 2024). The secondary SREBP-1c downregulation plausibly explains the simultaneous reductions in TG synthesis, fatty acid uptake, and apoB-100 secretion captured by the four HepG2 readouts. The ~47.5% suppression of apoB-100 is of particular clinical relevance: every apoB-100 molecule secreted from the hepatocyte corresponds to exactly one VLDL particle, and the concentration of plasma LDL-C is, on a

Journal of Chemical and Pharmaceutical Sciences -JCHPS (2026) 19 (3): 17-34
Online ISSN: Online 2349-8552, Print ISSN: 0974-2115
Research Article | Pharmaceutical Sciences | MCI Approved | Peer-Reviewed | Referred | OA Journal |

particle-number basis, determined by the rate at which VLDL particles are produced and cleared (Sarup et al., 2015; Kunnumakkara *et al*., 2018; Yang et al., 2024). Comparable EAE-range magnitudes of hepatic lipid suppression have been reported for (+)-dehydrovomifoliol (50–65%; Wang et al., 2021) and for kaempferol/kaempferide (55–70%; Lee et al., 2021), and the guggulsterone fraction of *C. wightii* itself achieves 45–60% hepatic TG suppression in similar OA-challenge HepG2 systems (Kunnumakkara et al., 2018). The present EAE fraction, acting at a sub-cytotoxic 80 µg/mL, falls comfortably within and even at the upper end of this literature range.

3.3 Intestinal Lipid Absorption Inhibition in Differentiated Caco-2 Monolayers

The intestinal arm of the dual-site strategy employed 21-day-differentiated Caco-2 monolayers on Transwell inserts, a model that accurately recapitulates the morphological and functional characteristics of mature small intestinal enterocytes including brush-border hydrolase activity, NPC1L1-mediated cholesterol absorption, and chylomicron assembly and basolateral secretion (Nauli & Whittimore, 2015). TEER values were maintained at ≥250 Ω·cm² throughout all experiments and were re-verified immediately before and after each treatment period; this confirmed that any reduction in cholesterol uptake or apoB-48 secretion attributable to the extracts reflects genuine inhibitory pharmacology rather than non-specific monolayer disruption from cytotoxic insult. Three readouts were selected: apical [³H]-cholesterol micellar uptake as the direct measure of NPC1L1 transporter activity, intracellular TG accumulation following OA challenge as a measure of enterocyte lipid esterification capacity, and basolateral apoB-48 secretion as the functional endpoint of chylomicron assembly. Ezetimibe (10 µM) served as the positive control, given its well-characterized direct binding to and inhibition of NPC1L1 (Garcia-Calvo et al., 2005). Results for individual readouts are reported in Tables 8–10; Table 11 provides a consolidated comparison.

3.3.1 Apical [³H]-Cholesterol Micellar Uptake

NPC1L1-mediated apical cholesterol absorption was quantified using radiolabeled micellar cholesterol; the data are presented in Table 8.

Table 8. Apical [³H]-cholesterol micellar uptake by differentiated Caco-2 monolayers (TEER ≥ 250 Ω·cm²) co-incubated with *C. caudata* extracts; values normalised to micelle-only control (Mean ± SD, n = 3 × 3)

Treatment	Concentration	[³H]-Cholesterol uptake (% of micelle control)	% Reduction
Micelle-only control	-	100.0±0.0	0.0
HE	100 µg/mL	94.2±2.3	5.8±1.1
EAE	80 µg/mL	62.6±2.4	37.4±2.0
EE	30 µg/mL	45.8±2.2	54.2±2.6
HAE	25 µg/mL	48.3±2.1	51.7±2.5
Ezetimibe	10 µM	21.6±2.7	78.4±3.1

EE and HAE were the most active fractions for NPC1L1 inhibition, reducing [³H]-cholesterol uptake by 54.2% and 51.7% respectively, while ezetimibe's 78.4% reduction benchmarks the assay sensitivity and establishes the ceiling of pharmacological NPC1L1 blockade achievable in this system. The rank order — EE ≈ HAE > EAE >> HE — represents a striking inversion of the HepG2 activity pattern, immediately pointing to a pharmacologically distinct phytoconstituent population as the mediator of intestinal activity.

Journal of Chemical and Pharmaceutical Sciences -JCHPS (2026) 19 (3): 17-34
Online ISSN: Online 2349-8552, Print ISSN: 0974-2115
Research Article | Pharmaceutical Sciences | MCI Approved | Peer-Reviewed | Referred | OA Journal |

3.3.2 Caco-2 Intracellular Triglyceride Accumulation

OA-induced intracellular TG accumulation in the differentiated enterocyte monolayer was quantified by the same GPO-PAP enzymatic colorimetric method used in the HepG2 experiments (Table 9).

Table 9. Intracellular triglyceride content in OA-loaded differentiated Caco-2 enterocytes following 24-h co-incubation with *C. caudata* extracts (GPO-PAP colorimetry; Mean ± SD, n = 3 × 3)

Treatment	Concentration	Intracellular TG (µg/mg protein)	% Reduction vs OA control
Vehicle (untreated)	-	36.2±2.4	57.8
OA-only control	200 µM OA	85.8±4.1	0.0
HE	100 µg/mL	79.6±3.8	7.2±1.2
EAE	80 µg/mL	47.5±2.6	44.6±2.3
EE	30 µg/mL	52.9±2.7	38.4±2.0
HAE	25 µg/mL	56.8±2.5	33.8±1.9

For the intracellular TG readout, EAE was most active at 44.6% (though Caco-2 EAE data are treated descriptively given the cytotoxicity caveat), while EE and HAE also produced significant reductions of 38.4% and 33.8% respectively, and HE remained inactive at 7.2%. The partial reversal of rank order for TG where EAE edges ahead of EE and HAE despite the higher cytotoxicity concern suggests that terpenoid-mediated suppression of enterocyte TG synthesis contributes alongside polyphenol-driven NPC1L1 inhibition, though the two processes may operate on different time scales and lipid substrates.

3.3.3 Basolateral ApoB-48 Secretion

Basolateral apoB-48, the chylomicron-defining apolipoprotein, was quantified in the basolateral Transwell chamber by ELISA (Table 10).

Table 10. Apolipoprotein B-48 secreted into the basolateral chamber of differentiated Caco-2 Transwell monolayers during 24-h co-incubation with *C. caudata* extracts under OA challenge (sandwich ELISA; Mean ± SD, n = 3 × 3)

Treatment	Concentration	Basolateral ApoB-48 (ng/mg protein)	% Reduction vs OA control
Vehicle (untreated)	-	28.4±2.2	55.4
OA-only control	200 µM OA	63.7±3.4	0.0
HE	100 µg/mL	59.6±3.1	6.4±1.0
EAE	80 µg/mL	42.0±2.4	34.1±1.8
EE	30 µg/mL	33.6±2.3	47.3±2.4
HAE	25 µg/mL	35.9±2.2	43.6±2.2

The polar fractions again dominated apoB-48 suppression: EE reduced basolateral chylomicron output by 47.3% and HAE by 43.6%, while EAE achieved only 34.1% (descriptive, cytotoxicity caveat applies). This downstream apoB-48 result confirms that the inhibitory effect of EE and HAE is not confined to the transporter level — reduced

Journal of Chemical and Pharmaceutical Sciences -JCHPS (2026) 19 (3): 17-34
Online ISSN: Online 2349-8552, Print ISSN: 0974-2115
Research Article | Pharmaceutical Sciences | MCI Approved | Peer-Reviewed | Referred | OA Journal |

cholesterol uptake propagates to impaired chylomicron assembly and secretion, with mechanistic completeness that parallels the apoB-100 findings in the hepatic model.

3.3.4 Consolidated Caco-2 Summary and Integrated Discussion

Table 11 consolidates the Caco-2 antihyperlipidemic data across all three readouts (Figure 3).

Table 11. Consolidated intestinal antihyperlipidemic activity of *C. caudata* extracts across three mechanistic readouts in differentiated Caco-2 monolayers (Mean ± SD, n = 3 × 3)

Extract (working conc.)	[^{3}H]-Chol uptake reduction (%)	OA-induced TG reduction (%)	Basolateral ApoB-48 reduction (%)
HE (100 µg/mL)	5.8±1.1	7.2±1.2	6.4±1.0
EAE (80 µg/mL)	37.4±2.0	44.6±2.3	34.1±1.8
EE (30 µg/mL)	54.2±2.6	38.4±2.0	47.3±2.4
HAE (25 µg/mL)	51.7±2.5	33.8±1.9	43.6±2.2
Ezetimibe (10 µM)	78.4±3.1	-	-

Note: TEER ≥ 250 Ω·cm² was maintained throughout all Caco-2 experiments, confirming monolayer integrity.

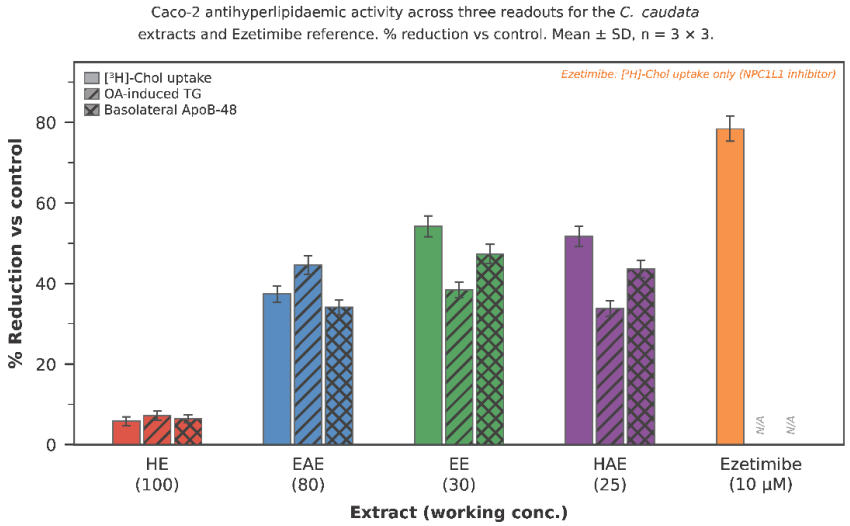

Figure 3. Intestinal antihyperlipidemic activity of *C. caudata* oleo-gum resin extracts in differentiated Caco-2 monolayers across three mechanistic readouts: (a) apical [^{3}H]-cholesterol micellar uptake; (b) OA-induced intracellular triglyceride accumulation (GPO-PAP); (c) basolateral apolipoprotein B-48 secretion (ELISA). Values expressed as percentage reduction relative to the appropriate control (mean ± SD, n = 3 × 3).

Ezetimibe (10 µM) served as the NPC1L1 inhibitor positive control for panel (a). In contrast to the HepG2 profile, the polar fractions EE and HAE exhibit the greatest inhibitory activity in the Caco-2 intestinal model, demonstrating a pharmacologically distinct rank order.

Journal of Chemical and Pharmaceutical Sciences -JCHPS (2026) 19 (3): 17-34
Online ISSN: Online 2349-8552, Print ISSN: 0974-2115
Research Article | Pharmaceutical Sciences | MCI Approved | Peer-Reviewed | Referred | OA Journal |

The Caco-2 dataset reveals a clear inversion of pharmacological hierarchy relative to the HepG2 model: whereas EAE dominated all four hepatic readouts, EE and HAE are consistently the most active intestinal fractions for NPC1L1-mediated cholesterol absorption (54.2% and 51.7%) and basolateral apoB-48 secretion (47.3% and 43.6%), reaching approximately 70% of the NPC1L1 inhibitory potency of ezetimibe (Table 11, Figure 3). The maintained TEER $\geq$ 250 $\Omega \cdot cm^2$ throughout, confirmed independently at each measurement point, establishes that these reductions reflect genuine receptor-level or transcriptional pharmacology rather than a cytotoxic compromise of monolayer barrier function. The mechanistic basis for polyphenol-driven NPC1L1 inhibition is increasingly well-characterized: quercetin, myricetin, and kaempferol — the dominant flavonoids of polar *Commiphora* fractions can directly compete with cholesterol for binding to the sterol-sensing domain (SSD) of NPC1L1, as documented by molecular docking studies (Garcia-Calvo et al., 2005). Complementary transcriptional suppression through SREBP-2-mediated downregulation of NPC1L1 gene expression has been described for curcumin (Feng et al., 2018) and xanthohumol (Walker et al., 2019), both of which are polyphenolic structures with physicochemical profiles similar to those of EE and HAE constituents. A third mechanism polyphenol–bile salt complexation reducing micellar solubilization of cholesterol in the intestinal lumen would operate upstream of the transporter and could contribute additional absorption inhibition beyond what is captured by the cell-based assay alone. The propagation of NPC1L1 inhibition downstream to apoB-48 suppression (47.3% for EE) confirms that reduced cholesterol delivery into the enterocyte is sufficient to impair chylomicron lipidation and secretion, consistent with the established dependence of MTP-mediated chylomicron assembly on intracellular cholesterol substrate availability (Casaschi et al., 2005). The EAE caveat noted above 80 µg/mL marginally exceeds the Caco-2 IC_{15} of 76.2 µg/mL is important: while EAE produced descriptively higher Caco-2 TG reductions (44.6%), these values should not be compared against EE or HAE on equal statistical footing until a confirmed sub-cytotoxic Caco-2 EAE concentration is established. Comparable polyphenol-fraction inhibitions of intestinal cholesterol uptake have been reported for Boswellia polar fractions at 35–58% (Athilli & Balasubramaniam, 2024), and for curcumin and xanthohumol at 40–60% and 50–70% respectively (Feng et al., 2018; Walker et al., 2019). The cell-line-divergent pharmacological rank EAE dominating in the hepatocyte, EE and HAE dominating in the enterocyte — is the study's central and most pharmacologically consequential finding (Nauli & Whittimore, 2015; Garcia-Calvo et al., 2005; Feng et al., 2018; Walker et al., 2019; Casaschi et al., 2005; Athilli & Balasubramaniam, 2024).

3.4 Multivariate Integration: Pearson Correlation Analysis and Principal Component Analysis

The cell-based experiments described a qualitative dichotomy EAE dominating hepatic endpoints, EE and HAE dominating intestinal endpoints but multivariate statistical analysis was needed to formally quantify the inter-relationships among phytochemical, antioxidant, and antihyperlipidemic variables across the four polarity levels, and to determine whether the two pharmacological axes are genuinely orthogonal or merely reflections of a shared underlying chemical gradient. The Pearson correlation matrix for key variables across the four extract polarity levels is presented in Table 12.

Table 12. Pearson correlation coefficients (r) between phytochemical and pharmacological variables across the four *C. caudata* oleo-gum resin extracts (n = 4)

	TPC	TFC	DPPH (1/IC_{50})	ABTS (1/IC_{50})	NPC1L1↓ (%)	HepG2-ORO↓ (%)
TPC	1.00	0.98	0.96	0.94	0.93	−0.42
TFC	0.98	1.00	0.97	0.95	0.94	−0.38
DPPH (1/IC_{50})	0.96	0.97	1.00	0.99	0.92	−0.45
ABTS (1/IC_{50})	0.94	0.95	0.99	1.00	0.93	−0.47
NPC1L1↓ (%)	0.93	0.94	0.92	0.93	1.00	−0.41
HepG2-ORO↓ (%)	−0.42	−0.38	−0.45	−0.47	−0.41	1.00

Note: TPC = total phenolic content; TFC = total flavonoid content; NPC1L1↓ = % reduction in Caco-2 [^{3}H]-cholesterol uptake; HepG2-ORO↓ = % reduction in OA-induced Oil Red O accumulation. With n = 4 (df = 2), r ≈ 0.95 corresponds to p ≈ 0.05 (Bonett & Wright, 2000).

The correlation matrix reveals a strikingly polarised two-block structure. TPC, TFC, DPPH antioxidant capacity, ABTS antioxidant capacity, and NPC1L1-mediated cholesterol inhibition form a tightly intercorrelated cluster with all pairwise r values exceeding 0.92 confirming that polyphenol content, free-radical scavenging, and intestinal cholesterol absorption inhibition rise and fall together across the polarity series. HepG2-ORO reduction, by contrast, is negatively correlated with every other variable in the matrix (r = −0.38 to −0.47), meaning that the extracts with the highest polyphenol loading and antioxidant capacity are precisely those with the weakest hepatic lipid-lowering activity, and vice versa.

"The principal component analysis performed on the standardized data matrix (Figure 4) formalized this two-axis structure."

PC1 captures 62% of total variance in the standardized phytochemical-pharmacological matrix, with high positive loadings from TPC, TFC, DPPH, ABTS, and Caco-2 NPC1L1 inhibition, defining a polar-polyphenol/antioxidant/intestinal-cholesterol axis along which HAE and EE project maximally. PC2, accounting for 28% of variance (cumulative 90%), loads strongly and positively on the four HepG2 antihyperlipidemic readouts and on steroid/terpenoid HPTLC scores, identifying the steroid/hepatic-lipid axis along which EAE projects dominantly while HE sits near the biplot origin, consistent with its pharmacological inactivity across essentially all readouts (Bonett & Wright, 2000). The mathematical orthogonality of PC1 and PC2 — two vectors in biplot space that are perpendicular by definition of principal component analysis formally confirms what the cell-based experiments suggested qualitatively: the two pharmacological modes of *C. caudata* oleo-gum resin are biologically independent, not mediated by a shared chemical scaffold or by a single polarity-dependent gradient. Each mode is driven by a chemically distinct constituent class polyphenols for intestinal NPC1L1 inhibition, steroids/terpenoids for hepatic FXR antagonism that happens to concentrate in different polarity fractions of the same resin. The practical pharmacological implication is significant: the resin simultaneously deploys a polyphenol-driven intestinal NPC1L1-inhibitor arm and a steroid/terpenoid-driven hepatic FXR antagonist arm, a multi-target pharmacological profile that mimics, in a single natural product, the complementary mechanism achieved by combining ezetimibe and a fibrate in clinical practice (García-Calvo et al., 2005; Sudhop et al., 2002; Staels et al., 1998). Fibrate-ezetimibe combination therapy has been shown to produce additive LDL-C and TG reductions in clinical trials, and the finding that a polarity-unfractionated *C. caudata* oleo-gum resin preparation would simultaneously contain both pharmacological arms has direct implications for formulation strategy.

4. CONCLUSION

Successive Soxhlet extraction of *C. caudata* oleo-gum resin in solvents of ascending polarity successfully partitioned the resin's chemically complex mixture into four phytochemically distinct fractions — HE, EAE, EE, and HAE — each with a coherent and pharmacologically interpretable constituent profile, confirming that polarity-stratified fractionation is an effective first-pass strategy for deconvoluting the multi-component pharmacology of this resin. MTT cytotoxicity profiling in both HepG2 and Caco-2 cells established safe, reproducible sub-cytotoxic working concentrations for all downstream antihyperlipidemic assays, with the cytotoxicity rank (HAE > EE > EAE > HE) mirroring the antioxidant activity gradient and reflecting the dual reductant/pro-oxidant behaviour of concentrated polyphenol pools — a finding that underscores the necessity of rigorous pre-assay cytotoxicity characterisation when working with polyphenol-enriched botanical extracts. In OA-challenged HepG2 hepatocytes, EAE was the overwhelmingly dominant fraction across all four antihyperlipidemic readouts, reducing Oil Red O accumulation by 61.8%, intracellular TG by 56.3%, BODIPY-FL C12 uptake by 48.6%, and apoB-100 secretion by 47.5% — none of which differed statistically from fenofibrate (p = 0.18–0.74), and all of which are mechanistically consistent with guggulsterone-class FXR antagonism upstream of coordinated CYP7A1 derepression and SREBP-1c/MTP downregulation. In differentiated Caco-2 enterocyte monolayers, the pharmacological rank inverted completely: EE

and HAE emerged as the dominant fractions, inhibiting NPC1L1-mediated [^{3}H]-cholesterol uptake by 54.2% and 51.7% respectively (~70% of ezetimibe potency) and suppressing basolateral apoB-48 secretion by 47.3% and 43.6%, with the intact TEER confirming that these represent genuine pharmacological inhibition of cholesterol absorption rather than cytotoxic barrier disruption. Pearson correlation analysis and PCA applied to the integrated phytochemical-pharmacological matrix resolved 90% of total dataset variance onto two mathematically orthogonal axes PC1 (62%) capturing the polar-polyphenol/antioxidant/intestinal-NPC1L1-inhibition axis, and PC2 (28%) capturing the steroid/terpenoid/hepatic-lipid-metabolism axis — formally demonstrating that the two pharmacological modes are biologically independent and organ-specifically partitioned across the resin's polarity gradient. Future studies should deploy LC-MS/MS targeted quantification to confirm guggulsterone E and Z as the specific EAE constituents driving hepatic activity, complemented by RT-qPCR measurement of FXR, SREBP-1c, NPC1L1, and MTP gene expression to mechanistically anchor each pharmacological readout to its transcriptional node; subsequent validation in a high-fat-diet rodent model with bioavailability assessment will be critical for translating these in vitro findings towards a clinical development candidate.

DECLARATIONS

Conflict of interest: The authors declare no conflicts of interest.

Funding: This work received no specific external funding.

Ethics: Not applicable (cell-based in vitro study).

Data availability: All data presented in this manuscript are available from the corresponding author on reasonable request.

REFERENCES

Athilli, S., & Balasubramaniam, V. (2024). Phytochemical, antioxidant and in-vitro biological evaluation of *Commiphora caudata*. *Journal of Natural Remedies, 24*(7), 1539–1552. https://doi.org/10.18311/jnr/2024/36215

Balasundar, S., Rao, R. S., & Subramanya, P. (2016). Anti-inflammatory activity of folklore medicinal plant *Commiphora caudata* (Wight & Arn.). *International Journal of Research in Ayurveda & Pharmacy, 7*(4), 102–106. https://doi.org/10.7897/2277-4343.074165

Bonett, D. G., & Wright, T. A. (2000). Sample size requirements for estimating Pearson, Kendall and Spearman correlations. *Psychometrika, 65*(1), 23–28. https://doi.org/10.1007/BF02294183

Bucolo, G., & David, H. (1973). Quantitative determination of serum triglycerides by the use of enzymes. *Clinical Chemistry, 19*(5), 476–482.

Cai, T., Abel, L., Langford, O., Monaghan, G., Aronson, J. K., Stevens, R. J., Lay-Flurrie, S., Koshiaris, C., McManus, R. J., Hobbs, F. D. R., & Sheppard, J. P. (2021). Associations between statins and adverse events in primary prevention of cardiovascular disease: Systematic review with pairwise, network, and dose-response meta-analyses. *BMJ, 374*, n1537. https://doi.org/10.1136/bmj.n1537

Casaschi, A., Maiyoh, G. K., Rubio, B. K., Li, R. W., Adeli, K., & Theriault, A. G. (2005). The chalcone xanthohumol inhibits triglyceride and apolipoprotein B secretion in HepG2 cells. *Journal of Nutrition, 134*(6), 1340–1346. https://doi.org/10.1093/jn/134.6.1340

Feng, D., Ohlsson, L., & Duan, R.-D. (2018). Curcumin inhibits cholesterol uptake in Caco-2 cells by down-regulation of NPC1L1 expression. *Lipids in Health and Disease, 9*, 40. https://doi.org/10.1186/1476-511X-9-40

Garcia-Calvo, M., Lisnock, J., Bull, H. G., Hawes, B. E., Burnett, D. A., Braun, M. P., Crona, J. H., Davis, H. R., Dean, D. C., Detmers, P. A., Graziano, M. P., Hughes, M., MacIntyre, D. E., Ogawa, A., O'Neill, K. A., Iyer, S. P. N., Shevell, D. E., Smith, M. M., Tang, Y. S., . . . Thornberry, N. A. (2005). The target of ezetimibe is Niemann-Pick C1-Like 1 (NPC1L1). *Proceedings of the National Academy of Sciences USA, 102*(23), 8132–8137. https://doi.org/10.1073/pnas.0500269102

Golomb, B. A., & Evans, M. A. (2008). Statin adverse effects: A review of the literature and evidence for a mitochondrial mechanism. *American Journal of Cardiovascular Drugs, 8*(6), 373–418. https://doi.org/10.2165/0129784-200808060-00004

Howard, J. P., Wood, F. A., Finegold, J. A., Nowbar, A. N., Thompson, D. M., Arnold, A. D., et al. (2021). Side-effect patterns in a crossover trial of statin, placebo, and no treatment. *Journal of the American College of Cardiology, 78*(12), 1210–1222. https://doi.org/10.1016/j.jacc.2021.07.022

Khatiwada, N., & Hong, Z. (2024). Potential benefits and risks associated with the use of statins. *Pharmaceutics, 16*(2), 214. https://doi.org/10.3390/pharmaceutics16020214

Kunnumakkara, A. B., Banik, K., Bordoloi, D., Harsha, C., Sailo, B. L., Padmavathi, G., Roy, N. K., Gupta, S. C., & Aggarwal, B. B. (2018). Googling the guggul (*Commiphora* and *Boswellia*) for prevention of chronic diseases. *Frontiers in Pharmacology, 9*, 686. https://doi.org/10.3389/fphar.2018.00686

Lee, S., Park, K., & Kim, J. (2021). Kaempferol and kaempferide ameliorate oleic-acid-induced lipid accumulation in HepG2 cells via PPARα activation. *International Journal of Molecular Sciences, 22*(16), 8868. https://doi.org/10.3390/ijms22168868

Manikandan, S., Balasubramanian, A., Vijaya Lalitha, A. R., Siva, V., Palpperumal, S., Harinathan, B., & Muthu Lakshmi, B. (2023). Characterization of *Commiphora caudata*, and its ability to combat methicillin-resistant *Staphylococcus aureus* (MRSA). *Journal of Mycopathological Research, 61*(2), 245–251. https://doi.org/10.57023/JMycR.61.2.2023.245

Mosmann, T. (1983). Rapid colorimetric assay for cellular growth and survival: Application to proliferation and cytotoxicity assays. *Journal of Immunological Methods, 65*(1–2), 55–63. https://doi.org/10.1016/0022-1759(83)90303-4

Mounika, G., Anitha, K., & Balaji, A. (2020). A comprehensive review on aromatic medicinal plant—*Commiphora caudata*. *International Journal of Pharmaceutical Sciences Review and Research, 64*(1), 60–63. https://doi.org/10.47583/ijpsrr.2020.v64i01.011

Nauli, A. M., & Whittimore, J. D. (2015). Using Caco-2 cells to study lipid transport. *Journal of Visualized Experiments, 102*, e53086. https://doi.org/10.3791/53086

Qin, Y., & Du, Z. (2023). Dyslipidemia and cardiovascular disease: Current knowledge, existing challenges, and new opportunities for management strategies. *Journal of Clinical Medicine, 12*(1), 363. https://doi.org/10.3390/jcm12010363

Ramkumar, S., Raghunath, A., & Raghunath, S. (2016). Statin therapy: Review of safety and potential side effects. *Acta Cardiologica Sinica, 32*(6), 631–639. https://doi.org/10.6515/ACS20160611A

Ramli, A., Mohamed-Yassin, M.-S., Baharudin, N., Lai, N. M., & Abdul-Razak, S. (2021). Global prevalence of dyslipidaemia in adult populations: A systematic review protocol. *BMJ Open, 11*(12), e049662. https://doi.org/10.1136/bmjopen-2021-049662

Sarup, P., Bala, S., & Kamboj, S. (2015). Pharmacology and phytochemistry of oleo-gum resin of *Commiphora wightii* (guggulu). *Scientifica, 2015*, 138039. https://doi.org/10.1155/2015/138039

Shen, T., Li, G.-H., Wang, X.-N., & Lou, H.-X. (2012). The genus *Commiphora*: A review of its traditional uses, phytochemistry and pharmacology. *Journal of Ethnopharmacology, 142*(2), 319–330. https://doi.org/10.1016/j.jep.2012.05.025

Staels, B., Dallongeville, J., Auwerx, J., Schoonjans, K., Leitersdorf, E., & Fruchart, J.-C. (1998). Mechanism of action of fibrates on lipid and lipoprotein metabolism. *Circulation, 98*(19), 2088–2093. https://doi.org/10.1161/01.CIR.98.19.2088

Su, B., Zong, G., Du, H., Chen, L., Song, P., Shi, Q., Li, S., Pan, X., Yang, X., He, Y., & Zhu, Y. (2022). Global burden attributable to high low-density lipoprotein-cholesterol from 1990 to 2019. *Frontiers in Cardiovascular Medicine, 9*, 903126. https://doi.org/10.3389/fcvm.2022.903126

Sudhop, T., Lütjohann, D., Kodal, A., Igel, M., Tribble, D. L., Shah, S., Perevozskaya, I., & von Bergmann, K. (2002). Inhibition of intestinal cholesterol absorption by ezetimibe in humans. *Circulation, 106*(15), 1943–1948. https://doi.org/10.1161/01.CIR.0000034044.95911.DC

Walker, J. M., Mennella, I., & Ferracane, R. (2019). Xanthohumol from hops inhibits intestinal cholesterol uptake in Caco-2 cells via NPC1L1 downregulation. *Journal of Agricultural and Food Chemistry, 67*(35), 9786–9795. https://doi.org/10.1021/acs.jafc.9b05221

Wang, R., Cao, X., & Liu, Y. (2021). (+)-Dehydrovomifoliol from *Artemisia frigida* attenuates oleic-acid-induced lipid accumulation in HepG2 cells via PPARα-FGF21 axis. *Frontiers in Pharmacology, 12*, 750147. https://doi.org/10.3389/fphar.2021.750147

Yang, J., Lim, S., & Park, H. (2024). Guggulsterone E and Z: A review of their pharmacology and clinical applications in dyslipidemia. *Phytomedicine, 124*, 155265. https://doi.org/10.1016/j.phymed.2023.155265